J. Phys. C: Solid State Phys., **15** (1982) 6613–6625. Printed in Great Britain

Phonon echoes in CdS and related piezoelectric semiconductors

J O Fossum and R M Holt†
Physics Department, Norwegian Institute of Technology, 7034 Trondheim NTH, Norway

Received 8 April 1982

Abstract. Wavevector-reversed phonon echoes in single crystals are generated by the interaction between a forward-propagating ultrasonic wave and an electric AC field. In piezoelectric semiconductors, the interaction consists of an electroacoustic (dielectric) and an electronic contribution. The latter is shown to be proportional to the conductivity in highly resistive crystals. This is demonstrated experimentally in CdS.

1. Introduction

The parametric interaction between a forward-propagating acoustic wave and an electric AC field is responsible for the generation of a backward acoustic wave, which is often termed a phonon echo. The existence of such a wavevector-reversed echo was originally suggested by Chaban (1967) in his discussion of nonlinear electroacoustics in semiconducting and insulating piezoelectrics. Svaasand (1969) performed an experiment where he detected the electric field formed by the mixing of two counterpropagating surface waves in $LiNbO_3$. Independently, the same effect was observed in CdS (Wang 1971). Thompson and Quate (1970) measured a backward-wave phonon echo in $LiNbO_3$ produced by the interaction of a shear wave with an electric field at the double frequency. Their work was partly motivated by the possibility of amplifying the forward wave by an electric pump field, in which they also succeeded. Simultaneously, Popov and Krainik (1971) observed backward-wave generation in the ferroelectric semiconductor SbSI by applying an electric field at the same frequency as that of the sound wave.

Phonon echoes were later observed in several materials (see, e.g., Fossheim and Holt 1982). The effect of wavevector reversal has recently been turned into a powerful tool for studying nonhomogeneous media (Shiren and Melcher 1978, Fossheim and Holt 1982), in particular in connection with phase transitions (Holt and Fossheim 1980, 1981, Fossheim and Holt 1980). Applications of the related effect of mixing two counterpropagating waves have been made in the field of signal processing (see, e.g., Luukkala and Kino 1971). SAW devices are constructed, utilising the fact that the interaction yields a convolved product of the input pulses.

Little effort has been put into research to establish a more profound understanding of the microscopic mechanisms responsible for echo generation. Shiren and Melcher

† Electronics Research Laboratory, Norwegian Institute of Technology, 7034 Trondheim NTH, Norway.

0022-3719/82/326613 + 13 $02.00

(1974) have presented a detailed theory describing the formation of ω,ω echoes† in piezoelectric semiconductors as well as three-pulse holographic storage echoes. The existence of $\omega,2\omega$ echoes in such materials did not follow from their theoretical outline. (Some aspects, especially the DC-field dependence, of $\omega,2\omega$ echo generation were later discussed by Economou and Spector (1978).) In this paper we discuss source terms of an electronic origin from which $\omega,2\omega/n$ echoes (n is an integer) may be generated. Our development is based on White's (1962) work on the electroacoustic effect in semiconductors. Similar treatments can be found in the theory for SAW convolvers with a semiconducting layer on a piezoelectric substrate (Otto 1974), and in the theory for mixing of acoustic waves in piezoelectric semiconductors (Conwell and Ganguly 1971).

Shiren *et al* (1973) studied ω,ω echoes in CdS, CdSe and CdTe (among others) at low temperatures. $\omega,2\omega$ echoes were also reported. Echoes with surface waves in CdS were investigated by Bastide *et al* (1978), while Yamamoto *et al* (1976) studied photoenhancement of convolution signals in a CdS/$LiNbO_3$ system. We have studied $\omega,2\omega$ echoes near room temperature, mainly in CdS. A few experiments have been performed with the related compounds CdSe and CdTe to give a qualitative description of the echo phenomenon in these crystals. The experimental results are given in § 4, together with a discussion based on the theoretical framework of § 2.

2. Theory

The constitutive relations for the mechanical stress T and the electric displacement D in a piezoelectric material can be written, to lowest (linear) order, as

$$T = cS - eE \tag{1}$$

$$D = \varepsilon E + eS. \tag{2}$$

Here $S = \partial u/\partial x$ is the mechanical strain (u is the particle displacement), E is the electric field and c, ε and e are the elastic, dielectric and piezoelectric constants respectively. Only one-dimensional wave propagation will be taken into account, so a scalar formalism will be used.

When phonon echo generation in *insulating* crystals is considered, higher-order terms have to be included in equations (1) and (2) in order to describe the effect. For instance, given the forward-propagating elastic wave

$$u^{\mathrm{F}} = u_0^{\mathrm{F}} \exp[-\mathrm{i}(\omega t - kx)] + \mathrm{cc} \tag{3}$$

and the applied electric field

$$E^{2\omega} = E_0^{2\omega} \exp(\mathrm{i}2\omega t) + \mathrm{cc}, \tag{4}$$

the backward-propagating echo

$$u^{\mathrm{B}} = u_0^{\mathrm{B}} \exp[\mathrm{i}(\omega t + kx)] + \mathrm{cc} \tag{5}$$

is given by the nonlinear mixing of u^{F} and $E^{2\omega}$. Expanding the elastic coefficient in a power series in the electric field, i.e. $c = c_0 + c_1 E + \ldots$, the echo amplitude is proportional to c_1:

$$u_0^{\mathrm{B}} \propto \tfrac{1}{8}(c_1/c_0) u_0^{\mathrm{F}} E_0^{2\omega}. \tag{6}$$

† The phonon echo is here labelled an 'ω_1,ω_2' echo, where ω_1 is the frequency of the initial sound wave and ω_2 is the frequency of the applied field.

$c_0 = c + e^2/\varepsilon$ is the piezoelectrically stiffened elastic constant. c_1 depends on the second-order piezoelectric, the electrostrictive and piezoelectric coefficients (see, e.g., Nelson 1979). When the shapes $\tilde{f}^{\mathrm{F}}$ and $\tilde{f}^{2\omega}$ of the input pulses are included, the resulting echo envelope $\tilde{f}^{\mathrm{B}}$ is a convolved product of $\tilde{f}^{\mathrm{F}}$ and $\tilde{f}^{2\omega}$ proportional to the lesser of the corresponding pulse widths Δt^{F} and $2\Delta t^{2\omega}$.

In piezoelectric semiconductors one may evaluate an expression similar to equation (6) replacing c_1 with $\tilde{c}_1$ where $\tilde{c}_1$ depends on the free-carrier concentration. Our experiments have been performed only with high-resistivity semiconductors. In these materials the number of free carriers is too small to have any influence on c_1; hence $\tilde{c}_1$ is independent of conductivity $\tilde{c}_1 \approx c_1$.

However, in the case of semiconductors, there is an additional contribution to the echo which can be evaluated from the linear equations (1) and (2). To show this, the effect of the conduction electrons in the nonlinear mixing of fields and strains must be considered (an n-type semiconductor is assumed for the sake of brevity).

The wave equation for a backward-propagating wave is

$$\rho \frac{\partial^2 u^{\mathrm{B}}}{\partial t^2} - c_0 \frac{\partial^2 u^{\mathrm{B}}}{\partial x^2} = \frac{eQn_{\mathrm{s}}^{\mathrm{B}}}{\varepsilon} \tag{7}$$

where $c_0 = c + e^2/\varepsilon$ and Poisson's equation

$$\partial D^{\mathrm{B}}/\partial x = -Qn_{\mathrm{s}}^{\mathrm{B}} \tag{8}$$

are inserted. The superscript B means backward-propagating Fourier components of the order $\exp[\mathrm{i}(\omega t + kx)]$ + CC of fields, strains or space-charge density n_{s}. Q is the elementary charge. The equation of charge continuity is

$$\partial n_{\mathrm{s}}/\partial t = Q^{-1}\, \partial J/\partial x. \tag{9}$$

The current density J contains both drift and diffusion contributions:

$$J = Q\mu n_{\mathrm{c}} E + QD_{\mathrm{n}}\, \partial n_{\mathrm{c}}/\partial x. \tag{10}$$

Here μ is the electron mobility and D_{n} is the diffusion constant. Further, the number of electrons in the conduction band is written as

$$n_{\mathrm{c}} = n_0 + f' n_{\mathrm{s}} \tag{11}$$

where n_0 is the equilibrium concentration and f' is the fraction of space charge present in the conduction band. $n_{\mathrm{c}} = n_0$ when no fields or waves are applied. $f' = 1$ in the case of no trapping. f' was considered theoretically by Greebe (1966). He showed that f' depends on the free-carrier density as well as the trap parameters in such a way that f' may approach unity when the electric conductivity is increased. Equations (9), (10) and (11) may be combined into a differential equation for n_{s}. From this $n_{\mathrm{s}}^{\mathrm{B}}$ is calculated:

$$n_{\mathrm{s}}^{\mathrm{B}} = \frac{e}{Q} \frac{\mathrm{i}\omega_{\mathrm{c}}/\omega}{\Gamma^{\mathrm{B}}} \frac{\partial S^{\mathrm{B}}}{\partial x} + \frac{\mu f'}{v_{\mathrm{s}}} \frac{n_{\mathrm{s}}^{2\omega} E^{\mathrm{F}} + E^{2\omega} n_{\mathrm{s}}^{\mathrm{F}}}{\Gamma^{\mathrm{B}}}. \tag{12}$$

Here Poisson's equation (8) is used, and the following definitions are introduced. $\omega_{\mathrm{c}} = \sigma/\varepsilon$ is the conductivity frequency, $\sigma = Q\mu n_0$ is the DC electric conductivity, $\omega_{\mathrm{D}} = v_{\mathrm{s}}^2/f' D_{\mathrm{n}}$ is the diffusion frequency, $v_{\mathrm{s}} = \omega/k$ is the sound velocity,

$$\Gamma^{\mathrm{B}} = \gamma^{\mathrm{B}} - \mathrm{i}\left(\frac{\omega_{\mathrm{c}}}{\omega} + \frac{\omega}{\omega_{\mathrm{D}}}\right),$$

$\gamma^B = 1 - (v_d/v_s)$, and $v_d = f'\mu E_0$ is the electron drift velocity. E_0 is an applied DC electric field and $E^{2\omega}$ and $n_s^{2\omega}$ are nonpropagating AC components of the electric field and the space-charge density, respectively ($\sim \exp(i2\omega t)$ + CC).

In equation (12), the term $n_s^{2\omega}E^F + E^{2\omega}n_s^F$ represents the source for n_s^B.

Equations (9)–(11) may also be solved with respect to the forward propagator

$$n_s^F = -\frac{e}{Q}\frac{i\omega_d/\omega}{\Gamma^F}\frac{\partial S^F}{\partial x} \tag{13}$$

where

$$\Gamma^F = \gamma^F + i\left(\frac{\omega_c}{\omega} + \frac{\omega}{\omega_D}\right)$$

and $\gamma^F = 1 + (v_d/v_s)$. Here the sources of order $n_s^{2\omega}E^B + E^{2\omega}n_s^B$ are neglected since S^F in this case represents the applied displacement wave u^F given in equation (3). Thus, S^F is the main source of n_s^F.

Equation (12) inserted into the wave equation (7) gives

$$\rho\frac{\partial^2 u^B}{\partial t^2} - c^B\frac{\partial^2 u^B}{\partial x^2} = \frac{eQ\mu f'}{\varepsilon v_s}\frac{1}{\Gamma^B}(n_s^{2\omega}E^F + E^{2\omega}n_s^F) \tag{14}$$

where

$$c^B = c\left(1 + K^2\frac{\gamma^B - i(\omega/\omega_D)}{\Gamma^B}\right)$$

is the complex elastic constant, from which the sound velocity and the attenuation can be found, in agreement with White's (1962) results. The attenuation is

$$\alpha = \frac{K^2}{2v_s}\omega\frac{\gamma\omega_c}{\omega}\left[\gamma^2 + \left(\frac{\omega_c}{\omega} + \frac{\omega}{\omega_D}\right)^2\right]^{-1} \tag{15}$$

where $K^2 = e^2/\varepsilon c$ is the electromechanical coupling constant and γ is γ^B or γ^F. Notice that with a DC field the forward and the backward waves are not equally damped. The right-hand side of equation (14) contains two source terms: the first term, $n_s^{2\omega}E^F$, was considered both from a theoretical and experimental point of view by Shiren and Melcher (1974) and Melcher and Shiren (1975). The echo generation in this case is due to the mixing of a forward-propagating strain wave S^F (or its associated field E^F) with a 2ω component in the space-charge density $n_s^{2\omega}$. Melcher and Shiren have discussed $n_s^{2\omega}$ in the case when both a nonpropagating AC field of frequency $2\omega/n$ (n is an integer) and a DC field E_0 are applied. They argue that when $E_0 = 0$, $n_s^{2\omega} \neq 0$ only for $n = 2, 4, 6, \ldots$, which means that the lowest-order echo in this case is an ω,ω echo. $\omega,2\omega$ echoes cannot be generated from this term when $E_0 = 0$. We choose $E_0 = 0$ and thus only have to take the second term $E^{2\omega}n_s^F$ into consideration. Further, assuming Im $c^B \ll$ Re c^B, and inserting n_s^F from equation (13) and α from equation (15), one arrives at the wave equation

$$\frac{1}{v_s^2}\frac{\partial^2 u^B}{\partial t^2} - \frac{\partial^2 u^B}{\partial x^2} = i\alpha\frac{2\mu f'}{\omega}E^{2\omega}\frac{\partial S^F}{\partial x}. \tag{16}$$

The $\omega,2\omega$ echo amplitude in a zero DC field can hence be written for a highly resistive sample:

$$u^B = \tfrac{1}{8}(c_1/c_0)u_0^F E_0^{2\omega}\omega\tilde{f}^B\sin(\omega t + kx) + \tfrac{1}{4}\mu f'\alpha u_0^F E_0^{2\omega}\tilde{f}^B\cos(\omega t + kx). \tag{17}$$

In equation (13) the $E^{2\omega}n_s^B$ contribution to n_s^F was neglected. This means that the force acting back on the forward wave during generation of u^B is not included. The displacement gain of the forward propagator u^F is clearly smaller than u^B. The power gain in each direction, however, is the same, and momentum conservation is satisfied. (See Baják's (1978) quantum-mechanical treatment of phonon echoes.)

In the conventional echo experiment, the echo, u^B, is detected at a time 2τ after applying the forward wave, u^F (τ is the delay time between the u^F pulse and the $E^{2\omega}$ pulse). Taking the attenuation of u^F and u^B into account, the conductivity-dependent part of the echo amplitude in equation (17) may be written as

$$u_0^B = \tfrac{1}{4}\mu f' \alpha u_0^F E_0^{2\omega} \tilde{f}^B \exp[-(\alpha_0 + \alpha)2v_s\tau] \tag{18}$$

where α_0 is the electron-independent part of the attenuation, while the electronic part $\alpha = (K^2/2v_s)\omega_c$ when $\omega_c/\omega \ll 1$ (highly resistive sample) and $\omega/\omega_D \ll 1$ is assumed. An expression similar to equation (18) can be obtained from the results of Economou and Spector (1978). Their approach is, however, different from ours. ($n_s^{2\omega} = 0$ and $f' = 1$ at the starting point of their calculations.)

It should be mentioned that including higher-order terms in equations (1) and (2) leads to new source terms for echo generation. For instance, there will be an additional term on the right-hand side of equation (15) which is proportional to $(\kappa eQ/\varepsilon)n_s^F E^{2\omega}$

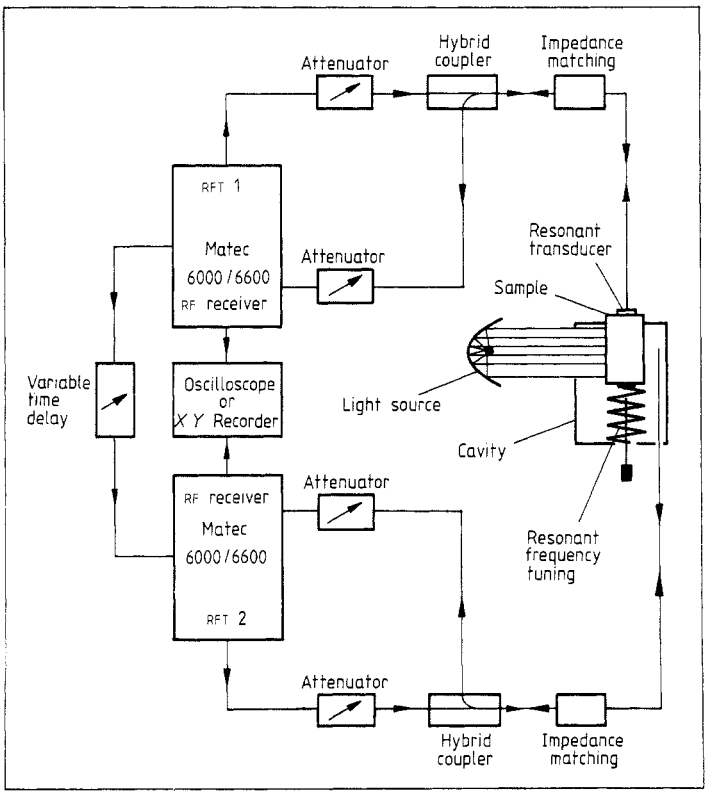

Figure 1. Experimental set-up for ultrasonic reflection and echo measurements. (RFT: RF transmitter.)

Table 1. Data for type-II–VI semiconductors (at room temperature).

	CdS	CdSe	CdTe
Crystal structure	Hexagonal	Hexagonal	Cubic
Sound velocity, v_s ($m\,s^{-1}$)	4470	3860	3020
Longitudinal waves ($\|c$ axis)			
Dielectric constant, $\varepsilon_{33}^S/\varepsilon_0$	9.5	10.2	11.0
Piezoelectric constants,			
e_{33} ($C\,m^{-2}$)	0.44	0.347	0
e_{14} ($C\,m^{-2}$)			0.30
Elastic constant, c_{33}^E ($N\,m^{-2}$)	$9.4 \times 10^{+11}$	$8.4 \times 10^{+11}$	5.4×10^{11}
Mobility, μ ($m^2\,V^{-1}\,s^{-1}$)	2×10^{-2}	5×10^{-2}	8×10^{-2}
Diffusion constant, $D_n = \mu kT/Q$ ($m^2\,s^{-1}$)	5.2×10^{-4}	12.9×10^{-4}	20.7×10^{-4}
$\omega_D = v_s^2/f' D_n$ (GHz) ($0 < f' < 1$)	>37	>11	>4

(Fossum *et al* 1981). κ is, like c_1, a sum of nonlinear electroacoustic coefficients. It can be shown that this contribution to the echo amplitude in high-resistivity semiconductors is roughly ω_c/ω smaller than the c_1 term. Hence it is not believed to play any significant role in the experimental results.

3. Experimental technique and samples

The experiments described in § 4 were performed using Matec equipment for RF transmitting and receiving, mostly in the frequency range 50–300 MHz. Figure 1 shows the experimental set-up. A $LiNbO_3$ transducer attached to one of the end faces of the sample generates the forward-propagating wave at frequency ω. The crystal is placed in the electric field of a helical resonant cavity which is tuned to 2ω (Fossheim and Holt 1978). The 2ω pulse is fired at a time τ and the backward-propagating echo is detected at 2τ. Light with tunable intensity is supplied from a white-light lamp either through a hole in the cavity wall or, in the case of low-temperature experiments, through a glass rod. The amplitudes of the signals detected (echo, and reflections between the end faces of the sample) were measured from the screen of an oscilloscope using calibrated attenuators. Alternatively an X–Y recorder and/or a Matec automatic attenuation recorder were used.

Type-II–VI semiconductor crystals of CdS, CdSe and CdTe were used in the experi-

Table 2. Samples used in the experiments.

Sample	Supplied from	Dark room $(\Omega\,cm)^{-1}$ conductivity	ω_c(dark) (MHz)	Direction of sound propagation
CdS I	IBM	Highly resistive		$\|c$ axis
CdS II	IBM	Highly resistive		$\|c$ axis
CdS III		4×10^{-11}	5×10^{-5}	$\|c$ axis
CdS IV	Cleveland Crystals Inc., Ohio	1.7×10^{-9}	2×10^{-3}	$\|c$ axis
CdSe	Cleveland Crystals Inc., Ohio	2×10^{-11}	2×10^{-4}	$\|c$ axis
CdTe	Cleveland Crystals Inc., Ohio	2×10^{-11}	2×10^{-4}	$\|(111)$ plane

ments. Some general crystal data are summarised in table 1, while the samples are described in table 2. All samples were highly resistive ($\omega_c/\omega \ll 1$) in darkness, and thus showed increasing sound attenuation with increasing illumination in agreement with equation (15). The CdS samples had different colours, indicating different impurity contents.

4. Experimental results and discussion

4.1. CdS

$\omega,2\omega$ phonon echoes were studied in all four CdS samples described in table 2. No DC field was applied during the experiments. The frequencies normally used were $\omega/2\pi =$ 90 MHz and $2\omega/2\pi = 180$ MHz. Thus (see table 1) $\omega \ll \omega_D$. The electronic part of the ultrasonic attenuation (equation (15)) can hence be written as

$$\alpha = \frac{K_2}{2v_s}\frac{\omega_c}{1+(\omega_c/\omega)^2}. \tag{19}$$

Since $\omega_c = \sigma/\varepsilon$, the attenuation at a given frequency will increase with increasing photoconductivity up to a maximum at $\omega_c = \omega$. Above this, α decreases as $1/\omega_c$. At 90 MHz, an increased absorption was seen in all the samples during illumination. Lowering the frequency to 30 MHz, the maximum could be reached at the highest available light intensity. For all the data presented here $\omega_c/\omega \leqslant \frac{1}{3}$ is valid.

Experimentally, the phonon echo amplitude was normally found to increase under illumination. This can be explained by inspecting equation (18), from which the echo depends on the conductivity (e.g illumination) through $\alpha(=(K^2/2\varepsilon v_s)\sigma)$ and through the trap factor f'. At moderate levels of light intensity and short intervals τ, the echo is proportional to α. Increasing the light intensity further, however, leads to a decay of the echo because of the absorption factor $\exp(-\alpha v_s 2\tau)$. This is confirmed qualitatively for all the CdS samples described in table 2.

Figure 2 shows an $\omega,2\omega$ echo generated in sample CdS I at room temperature. The sample is illuminated with intense white light amplifying both the echo and the ultrasonic attenuation. The resulting echo amplitude is about 10 dB larger than the first reflected pulse. In the other samples it was in fact possible to damp out all the reflections, studying echoes generated within $\tau < L/v_s$ (L is the length of sample). In darkness, the echo signal was comparable with the noise. Hence an increase of about 100 dB is achieved by the illumination.

A more quantitative description of the light sensitivity of the echo is given in figure 3. The ratio between the illuminated echo (u^B) and the echo in darkness (u^B(dark)) is plotted for three different samples as a function of the increase $\Delta\alpha$ in ultrasonic attenuation. $\Delta\alpha$ is measured directly from the reflected pulse train of the initial wave, so the attenuation measurements are here used as a method to study the bulk conductivity changes in the same path as is travelled by the phonon echo. Notice that $\Delta\alpha$ is sometimes so small that it has to be measured at reflected pulses far out in the train, which yields some uncertainty due to interference effects. However, disregarding the absorption of the echo itself, the ratio u^B/u^B(dark) can be written (from equation (17)) as

$$\left|\frac{u^B}{u^B(\text{dark})}\right| = 1 + \frac{\Delta\alpha}{\alpha(\text{dark}) + (c_1\omega/2c_0\mu f')}. \tag{20}$$

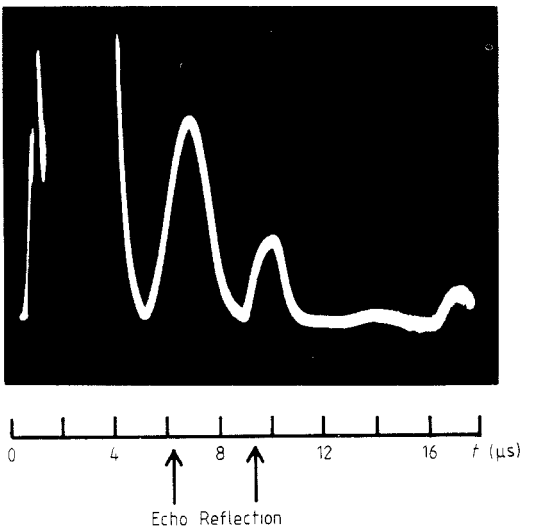

Figure 2. $\omega,2\omega$ echo signal (signal-to-noise ratio ~100 dB) and first reflection in the CdS I sample at room temperature. Frequency $\omega/2\pi = 90$ MHz.

Here the total attenuation is split into a light-sensitive part $\Delta\alpha$ and an attenuation coefficient in darkness, α(dark). The electron-independent part of the echo is taken from equation (6).

The results in figure 3 are in accord with the straight-line behaviour predicted from equation (20). The slopes of the lines are given by the inverse of the denominator. α(dark) is known in sample CdS III only and is much smaller than the inverse slope, which then must be equal to $(2c_0/c_1\omega)\mu f'$ in this case. Thus the different slopes obtained in figure 3 are most likely due to the sample-dependent factor $\mu f'$.

No results for the CdS IV crystal are included in figure 3. This is because the sound absorption in this sample is so light sensitive that all signals are rapidly damped out.

Figure 4 shows X–Y recorder plots of u^B as a function of $\Delta\alpha$ under varying white-

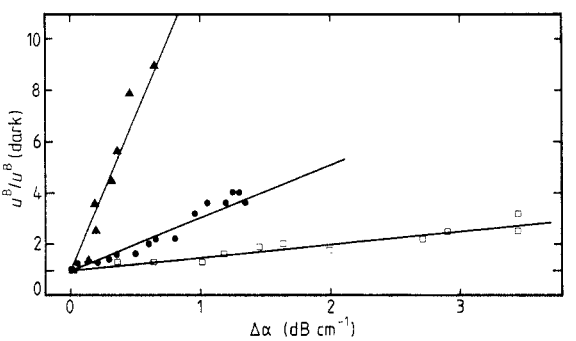

Figure 3. $\omega,2\omega$ echo amplitude, u^B, normalised to its value in darkness, u^B(dark), as a function of the increase in ultrasonic attenuation, $\Delta\alpha$, for three different samples at room temperature: ▲, CdS I; ●, CdS II; □, CdS III. Sound frequency $\omega/2\pi = 90$ MHz. The samples were illuminated with white light.

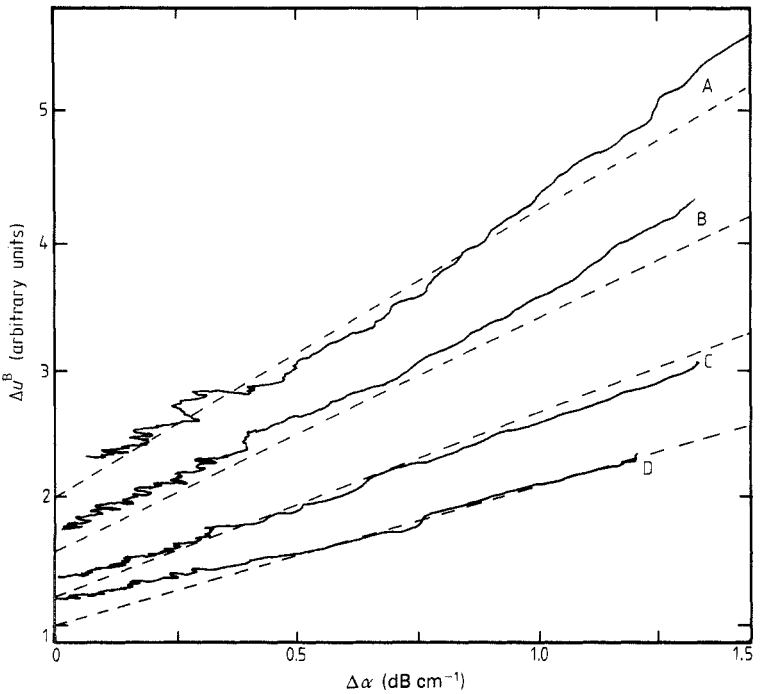

Figure 4. *X–Y* recorder plots showing photoenhancement of $\omega,2\omega$ echo amplitude, u^B, as a function of the increase in ultrasonic attenuation, $\Delta\alpha$, for four different magnitudes of the 2ω field for sample CdS I at room temperature: A, 0 dB; B, −2 dB; C, −4 dB; D, −6 dB. The broken lines are theoretical predictions. Sound frequency $\omega/2\pi = 90$ MHz.

light illumination. Plots are made for different values of the 2ω field amplitude $E_0^{2\omega}$, which according to equation (18) yields lines of different slopes with a linear dependence $u^B \propto E_0^{2\omega}$. The agreement between theory and experiment is very good. Given one of the lines in the figure, all the others can be calculated immediately. It should be stressed that we have assumed that f' does not play any important role in the light amplification of the echo. Further, the requirement that the echo absorption can be neglected demands that $\Delta\alpha < 2$–5 dB cm^{-1} when τ is chosen in the region 2–5 μs.

Equation (18) predicts a linear dependence of $E_0^{2\omega}$, u_0^F and the lesser of Δt^F and $2\Delta t^{2\omega}$ through the shape function $\tilde{f}^B$. In sample CdS III this is fully confirmed. In the other samples, however, additional nonlinear effects of field amplitudes and pulse widths are obtained. The echo amplitudes are also seen to depend on the RF repetition rate. These effects are most distinct in the CdS I sample, as shown in figure 5, where the echo amplitude is measured as a function of the 2ω electric field amplitude in samples I and III.

These effects are not stable; that is, they die out after some time. An example is shown in figure 6, where at time zero the RF repetition rate is suddenly increased by a factor 10 and kept constant thereafter. The echo amplitude at first increases relatively fast, but then slowly decreases to its original value after about two hours.

Curves similar to figure 6 may also be obtained by suddenly increasing u_0^F, $E_0^{2\omega}$, Δt^F or $\Delta t^{2\omega}$. Figure 7 shows different *X–Y* recordings of u^B against $\Delta\alpha$ for sample CdS I. The recordings are similar to figure 4, but in this case u^B and α are changed, varying four different parameters, namely illumination intensity, acoustic wave amplitude u_0^F, 2ω

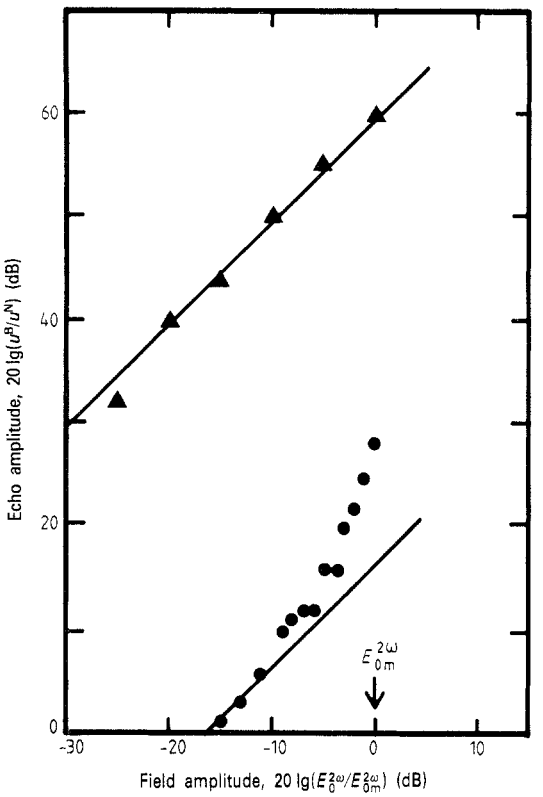

Figure 5. ω,2ω echo amplitude (signal (u^B)-to-noise (u^N) ratio) as a function of the 2ω electric field amplitude for two samples at room temperature (●, CdS I; ▲, CdS III), showing deviation from linear dependence in one sample. $\omega/2\pi = 90$ MHz.

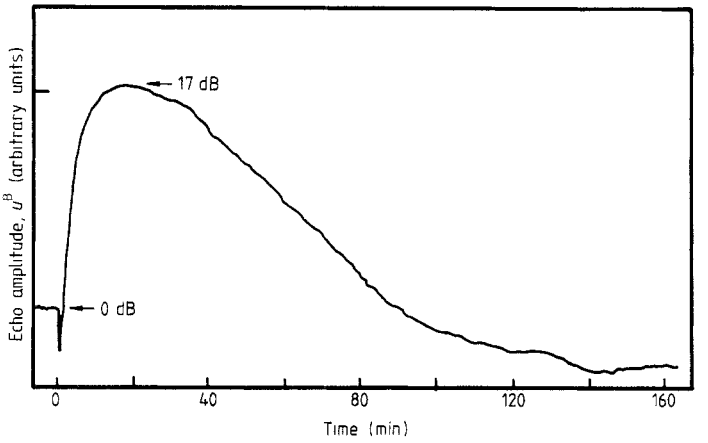

Figure 6. Time development of echo amplitude, u^B, in sample CdS I after sudden increase of RF pulse repetition rate, RR, from 320 PPS to 3200 PPS at time zero. Sound frequency $\omega/2\pi = 90$ MHz. Room temperature.

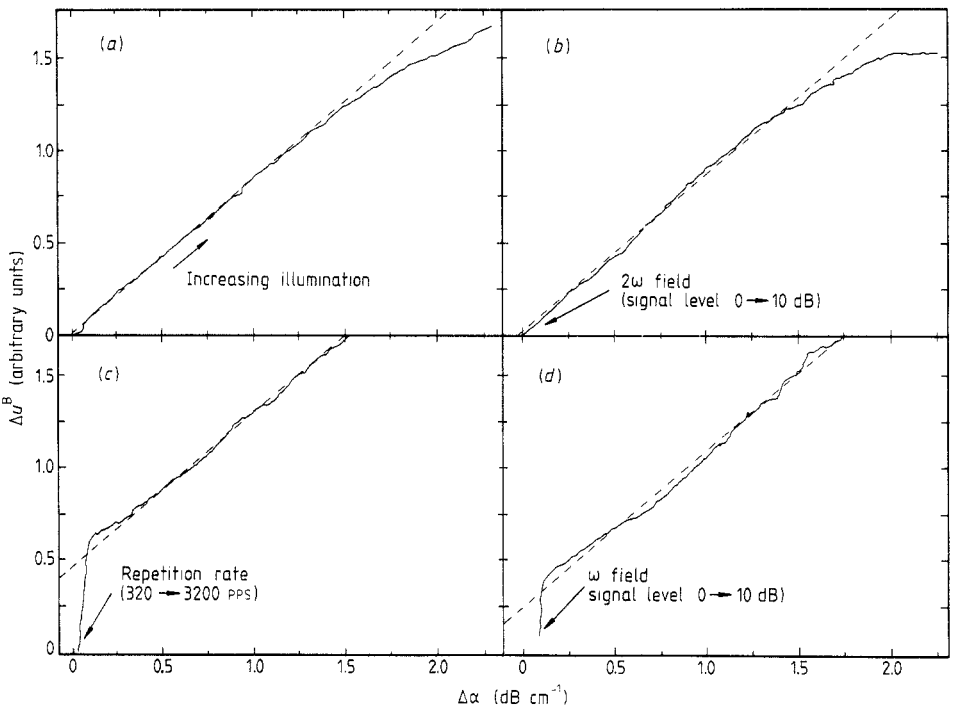

Figure 7. ω,2ω echo amplitude, Δu^B, as a function of ultrasonic attenuation, $\Delta\alpha$, for sample CdS I at room temperature. $\omega/2\pi = 90$ MHz. The enhancement of Δu^B and the simultaneous increase in $\Delta\alpha$ is due to (*a*) white-light illumination, (*b*) a sudden increase (similar to figure 6) of the 2ω field, (*c*) RF pulse repetition rate and (*d*) ω field amplitude. The slopes of the straight lines (broken) are the same in all cases as predicted from the theory.

field amplitude $E_0^{2\omega}$ and RF repetition rate RR. u_0^F, $E_0^{2\omega}$ and RR are instantly changed from a small value. Then the recorder has been running for some time while the echo amplitude has followed a curve like that shown in figure 6. All four experiments in figure 7 yielded the same straight line, indicating that the four parameters amplify the echo (mainly) through the conductivity. The first steep increase for two curves may be due to the trap factor f'. The deviation from straight-line behaviour at high illumination level (large $\Delta\alpha$) can be explained by the attenuation factor $\exp[-(\alpha_0 + \alpha)2v_s\tau]$ in equation (18).

All measurements discussed so far were performed at room temperature. Experiments throughout the region 77–350 K with white-light illumination indicate that the echo generation is linearly dependent on the electric conductivity at all temperatures. A complicating factor in mapping the temperature dependence of the phonon echo is that the critical fields u_0^F and E_0^2 are temperature dependent (through the acoustic bond, the dielectric constants of transducer and sample, etc). However, it seems that conductivity changes due to different impurity levels in the samples are the most important feature in the temperature dependence of the echo. Due to a lack of knowledge of the impurity content, this point has not been analysed any further.

4.2. CdSe

A few experiments were performed with longitudinal sound waves and the electric 2ω

field along the c axis in CdSe. Echo amplitudes about 40–50 dB above noise level were measured in darkness at room temperature. Under illumination, the absorption did not change significantly, which means that the electronic conductivity is rather insensitive at the light intensities available. The observed echo decreased, however. This effect can be fully attributed to a reduction in the cavity field: the illumination decreases the Q factor of the loaded cavity by increasing the dielectric loss factor. A change in Q from about 60 to about 15 was observed as the white-light intensity was increased from zero to maximum. (This effect could hardly be seen in the CdS experiments.) It is therefore conceivable that the observed echo is caused by purely dielectric and electroacoustic nonlinearities, that is the first term in equation (17). It is thus the same kind of echo as is found in insulating piezoelectrics. As in these materials, a bilinear field dependence $u_0^B \propto u_0^F E_0^{2\omega}$ was observed. Further, no dependence on the repetition rate could be seen. The echo did not change with temperature in the region 150–300 K.

Since only one sample was available during the present experiments, it is not clear whether light-amplified echoes can be observed in CdSe.

4.3. CdTe

In CdTe also echoes of 20–30 dB could be detected in darkness at room temperature. The ultrasonic waves were propagated in the (111) plane, where there is a piezoelectric coupling for longitudinal modes. Illumination increased the echo by 10–15 dB. The attenuation was also weakly influenced by the light applied externally, but the quality of the pulse train was too poor to allow any quantitative investigation of the echo properties. The results may indicate that in the present sample the echo is amplified by the illumination mainly through the trap factor f' in addition to a minor conductivity dependence, but there is also an intrinsic echo effect as in insulating crystals. Notice that there is a long-time dependence in the echo properties which has not been studied in detail here.

5. Concluding remarks

Phonon echoes in piezoelectric semiconductors can be of a combined nonlinear electroacoustic and electronic origin. The electronic part of the echo consists of two source terms, $n_s^{2\omega}E^F + E^{2\omega}n_s^F$. For $\omega,2\omega$ echoes, $n_s^{2\omega} = 0$, so the observed echoes are due to the latter term. The forward-propagating space-charge density n_s^F was calculated in § 2, and the resulting echo turns out to be proportional to the electronic conductivity. This may also explain why Melcher and Shiren (1975) did not observe $\omega,2\omega$ echoes in CdS without an external DC bias field at 4.2 K, where the conductivity is diminishingly small. ω,ω echoes also may originate from $n_s^{2\omega}E^F$, which is not proportional to the conductivity and hence may be of major importance at low temperature.

Experimentally, the echo in CdS was found to behave in proportion to the acoustic absorption, which from theory (White 1962) is a measure of the bulk conductivity. This linear relationship was confirmed through varying several parameters such as the white-light illumination intensity, the RF pulse repetition rate, the field amplitudes and pulse widths.

In CdSe and CdTe, we found that the purely electroacoustic part of the echo was more dominant, but in CdTe there is in addition a conductivity-dependent part.

Acknowledgments

The authors wish to acknowledge Professor Kristian Fossheim for his interest in the present work and Haakon J Aune who was involved in some of the experiments.

References

Baják I L 1978 *Phys. Rev.* B **18** 2405
Bastide G, Sagnes G and Rouzeyre M 1978 *J. Physique* **39** 1299
Chaban A A 1967 *JETP Lett.* **6** 381
Conwell E M and Ganguly A K 1971 *Phys. Rev.* B **4** 2535
Economou J E and Spector H N 1978 *Phys. Rev.* B **18** 5578
Fossheim K and Holt R M 1978 *J. Phys. E: Sci. Instrum.* **11** 892
—— 1980 *Phys. Rev. Lett.* **45** 730
—— 1982 *Physical Acoustics* vol. 16 ed. W P Mason and R N Thurston (New York: Academic)
Fossum J O, Fossheim K, Aune H J and Holt R M 1981 *J. Physique* C **6** 867
Greebe C A A J 1966 *IEEE Trans. Sonics and Ultrasonics* **SU-13** 54
Holt R M and Fossheim K 1980 *Ferroelectrics* **25** 515
—— 1981 *Phys. Rev.* B **24** 2680
Luukkala M and Kino G S 1971 *Appl. Phys. Lett.* **18** 393
Melcher R L and Shiren N S 1975 *Phys. Rev. Lett.* **34** 731
Nelson D F 1979 *J. Physique* C **8** 149
Otto O W 1974 *J. Appl. Phys.* **45** 4373
Popov S N and Krainik N N 1970 *Sov. Phys.–Solid State* **12** 2440
Shiren N S and Melcher R L 1974 *IEEE Ultrasonics Symp. Proc.* p 558
—— 1978 *Phonon Scattering in Solids* ed L J Challis, V W Rampton and A F G Wyatt (New York: Plenum) p 405
Shiren N S, Melcher R L, Garrod D K and Kazyaka T G 1973 *Phys. Rev. Lett.* **31** 819
Svaasand L O 1969 *Appl. Phys. Lett.* **15** 300
Thompson R B and Quate C F 1970 *Appl. Phys. Lett.* **16** 295
Wang W C 1971 *Appl. Phys. Lett.* **18** 337
White D L 1962 *J. Appl. Phys.* **33** 2547
Yamamoto H, Tsubouchi K, Minagawa S and Mikoshiba N 1976 *IEEE Ultrasonics Symp. Proc.* p 179